Article

High-Conductive Multilayer TiO$_X$-Ti$_3$C$_2$T$_X$ Electrocatalyst for Longevous Metal-Oxygen Battery under a High Rate

Zhihui Sun [ID], Shuai Zhao * and Jixiong Zhang *

School of Mines, China University of Mining and Technology, Xuzhou 221116, China
* Correspondence: zhaoshuai6074@cumt.edu.cn (S.Z.); zjxiong@163.com (J.Z.)

Abstract: Metal-oxygen batteries (especially Li-O$_2$ battery) with ultrahigh theoretical energy density are of great promise for long-range vehicle electrification. However, the limited enduring stability and low-rate property further restricted the large-scale commercial application of metal-oxygen batteries. We firstly report the fabrication of a TiO$_X$@Ti$_3$C$_2$T$_X$ with multilayer structure and its utilization as cathode for Li-O$_2$ batteries. The TiO$_X$ protective layer was fabricated in situ to directly optimize surface properties of Ti$_3$C$_2$T$_X$, as well as to strengthen surface active functional groups. The initial discharge capacity of as-prepared TiO$_X$@Ti$_3$C$_2$T$_X$ cathode reaches 7100 mAh g^{-1} at 2500 mA g^{-1}, as well as delivers impressive cycling stability (>100 cycles) at 2500 mA g^{-1}. Experimental analysis reveals that the in situ TiO$_X$ protective layer enhanced active functional-groups and the improved complete decomposition of discharge products Li$_2$O$_2$ are three critical factors for promoting the electrochemical performance of LOBs. This work exhibits a new insight into the design of MXene electrocatalysts for metal-oxygen batteries.

Keywords: Ti$_3$C$_2$T$_X$; TiO$_X$ protective layer; active functional-groups; bifunctional electrocatalysts; Li-O$_2$ battery

1. Introduction

Under the threat of serious environmental pollution and energy crisis, energy storage and conversion technologies have attracted extensive worldwide attention [1–3]. Due to the ultra-high theoretical energy density, lithium-oxygen batteries (LOBs) have been considered as a competitive candidate for next generation electrochemical energy storage devices [4,5]. Major obstacles to the practical application of LOBs are the limited enduring stability, large polarization, and low-rate capability, which could be ascribed to the sluggish dynamics of oxygen reduction reaction and oxygen evolution reactions (ORR and OER) [6,7]. To this end, great efforts have been devoted to solve the above-mentioned challenges in recent years, mainly including the synthesis of high-efficiency dual-functional catalysts [8,9], the exploration of stable electrolytes [10,11], Li-anode modification engineering [12,13], and the fabrication of selective membrane [14,15]. It is noted that efficient bifunctional catalyst with high stability is of paramount significance to promote the sluggish kinetics of ORR and OER both occurring on the cathode [16,17].

Recently, carbonaceous materials, noble metals, metal oxides, metal sulfides, and compound matrices have already been intensively investigated as promising catalysts for LOBs [18,19]. Nevertheless, noble metals deliver high capacity and low overpotential, but are hindered by high cost and low reserves [20,21]. Carbonaceous materials are characterized by high conductivity, large surface area, and easy chemical functionalization, which are widely applied practically in electrochemical energy storage [22,23]. Carbon tends to be easily oxidized at high potentials and oxygen-rich organic environment, resulting in poor cycling lifespan and high voltage polarization [24]. Besides, the indistinctive electrochemical property and poor adjustability of metal oxides needs to be addressed urgently [25,26].

Impressively, featured by superior physical/chemical stability, tunable structure/properties, and excellent conductivity (~9880 S cm^{-1}), Ti$_3$C$_2$T$_x$ MXene (where T$_x$ represents various surface terminations) are already widely applied in nitrogen reduction, hydrogen evolution, carbon dioxide reduction, and batteries [27–29]. With unique flexible layered structure and high tensile strength, Ti$_3$C$_2$T$_x$ can act as a conductive matrix, which could significantly reduce ion diffusion barrier and tolerate a large volume change derived from the deposition of Li$_2$O$_2$ in LOBs [30,31]. The abundant active functional groups (-O, -F, -OH, etc.) on the surface of Ti$_3$C$_2$T$_x$ can be served as fine catalytic active sites to promote the adsorption and desorption ability of discharge products, thus optimizing the kinetics [32]. Song et al. introduced lithium ions into the layered structure of Ti$_3$C$_2$T$_x$ by electrostatic interaction and successfully optimized the O termination groups [33]. Furthermore, the synergistic effect between uniform O-terminal surface and abundant intercalated Li$^+$ could provide remarkable stable catalytic sites (=O, Li$^+$) and enhanced structural stability for Ti$_3$C$_2$T$_x$, leading to high electrochemical performance. Il-Kwon Oh and co-worker also synthesized Ti$_3$C$_2$T$_x$ MXene with carboxylic acid graft, which showed superior electrocatalytic properties for ORR and OER due to the formation of metalloporphyrin structure and unpaired electrons [34]. Interestingly, Long et al. prepared in situ vacancy-rich TiO$_2$ nanoparticles on Ti$_3$C$_2$T$_x$ nanosheets by applied thermodynamic metastable Ti atoms as nucleation sites, achieving good rate capability and cycle stability in LOBs [35]. However, Ti$_3$C$_2$T$_x$ MXene is extremely unstable in oxygen-rich environments (especially O^{2-}, O$^-$ in LOBs) and gradually transforms into an undesired passivation layer (TiO$_2$) on the surface. As a result, Ti$_3$C$_2$T$_x$ MXene always suffer due to weakened electrocatalytic activity [36,37]. Therefore, how to design active Ti$_3$C$_2$T$_x$ with high-durability remains a great challenge.

Herein, we reported a facile in situ surface engineering to form a TiO$_X$ protective layer on Ti$_3$C$_2$T$_X$ by one-step hydrothermal reaction for the first time. The TiO$_X$ protective layer was adopted to directly optimize surface properties of Ti$_3$C$_2$T$_X$, as well as to strengthen surface active functional groups, thus improving the electrochemical activity and stability of Ti$_3$C$_2$T$_X$. The LOBs based on TiO$_X$-Ti$_3$C$_2$T$_X$ cathode exhibit superior specific capability (7169 mAh g^{-1}) and endurable stability at ultra-high rate (2500 mA g^{-1}). Further analysis indicates that TiO$_X$@Ti$_3$C$_2$T$_X$ could promote fast charge transfer kinetics and the decomposition of insoluble discharge products. This work provides a new and easy way to improve the stability and electrochemical activity of MXene catalysts for LOBs.

2. Materials and Methods

2.1. Synthesis of TiO$_X$-Ti$_3$C$_2$T$_X$

One gram of lithium fluoride was dissolved in 20 mL hydrogen chloride (9 M) solution with magnetic stirring for 30 min. Then, 1 g Ti$_3$AlC$_2$ powder was slowly dropped into the above solution under vigorous stirring for 30 min. The mixture was sealed in a 50 mL PTFE-lined stainless-steel autoclave and heated at 90 °C for 24 h. The resultant was centrifuged with deionized water and ethanol at 10,000 rpm for 5–6 times until the pH value was adjusted to ~6. Finally, the collected precipitate was dried at 60 °C and was calcined at 300 °C for 2.5 h.

2.2. Electrochemical Measurement

The as-prepared sample was evenly sprayed onto the carbon paper (ϕ = 13 mm) with mass loading of 0.6 $\pm$ 0.1 mg cm^{-2} to mark it as the cathode. Furthermore, 1 M lithium bis (trifluoromethane sulfonamide, LiTFSI) was dissolved in dimethyl sulfoxide, the resulting solution acted as an electrolyte. The lithium metal foil with diameter of 16 mm was chosen as the anode. The LOBs were prepared and assembled in a glove box filled with Ar. The assembled LOBs were measured by LAND CT 3001A to test the electrochemical performance. The electrochemical impedance spectroscopy was carried out by CHI 1600E.

3. Results

The preparation of TiO_X-$Ti_3C_2T_X$ is illustrated in Figure 1a. Briefly, TiO_X-$Ti_3C_2T_X$ could be successfully obtained by one-step hydrothermal treatment acting as a simple acid etching. SEM analysis was performed to characterize the morphologic changes of the sample in Figures 1b and S1. After acid etching activation, MAX was successfully stripped into a multilayer sheet structure to provide greater contact area and expose more active sites. The XRD patterns of as-prepared samples are shown in Figure 1c. The peaks of the MAX are identical to the Ti_3AlC_2, which is consistent with a previous report. After etching, the peak located at 39° attributed to the typical Ti_3AlC_2 (104) plane disappears, indicating that the Al layer has been selectively removed. The FTIR spectra of MXene (TiO_X-$Ti_3C_2T_X$) and MAX (Ti_3AlC_2) are shown in Figure 1d. The sharp peaks at 669, 1630, and 3480 cm^{-1} are consistent with the functional groups' stretching vibrations (C-O, -COOH, -OH). Impressively, the intensity of these functional groups is significantly enhanced, and a new peak representing the Ti-O bond (559 cm^{-1}) appears after the hydrothermal modification, indicating that a new layer of titanium oxide and a variety of active functional groups are fabricated on the surface of $Ti_3C_2T_X$.
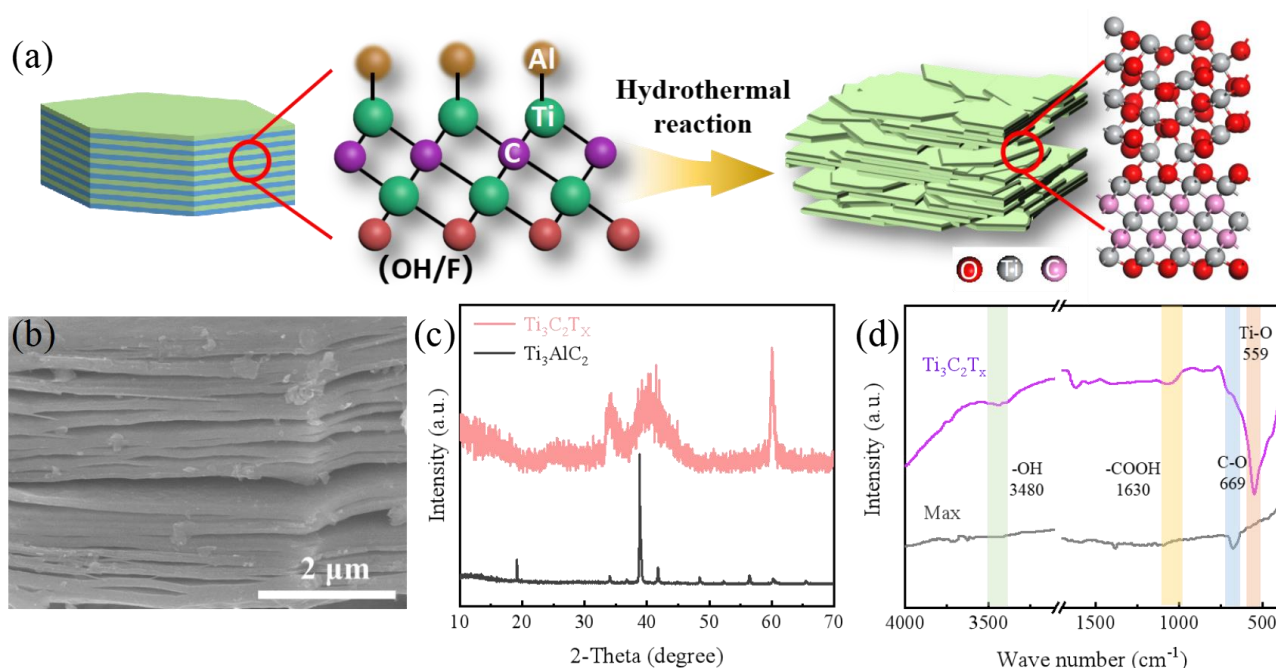

Figure 1. (**a**) Schematic description of the preparation of TiO_X-$Ti_3C_2T_X$; (**b**) SEM image of TiO_X-$Ti_3C_2T_X$; XRD patterns (**c**) and FTIR curve (**d**) of as-prepared samples.

The TEM image (Figure 2a,b) shows TiO_X-$Ti_3C_2T_X$ with a uniform multilayer sheet structure. The corresponding SAED pattern (Figure 2b inset) obviously exhibits the co-existence of (002), (110) planes of $Ti_3C_2T_X$. The HRTEM image (Figure 2c,d) clearly demonstrates interplanar spacing of 0.253 nm and 0.234nm, related to (110) plane of $Ti_3C_2T_X$ and (004) plane of TiO_2, respectively [38,39]. Interestingly, there are also considerable amorphous structures near the TiO_2 crystalline phase. This phenomenon could be ascribed to the fact that the TiO_2 layer is of hybrid amorphous/crystalline structure. The corresponding EDS mappings (Figure 2e) show that Ti, O, and C elements are evenly distributed across the surface of TiO_X-$Ti_3C_2T_X$. Besides, as shown in Figure S2 and Table S1, there is obviously no Al element present on the surface of TiO_X-$Ti_3C_2T_X$, indicating that the Al has been selectively removed.

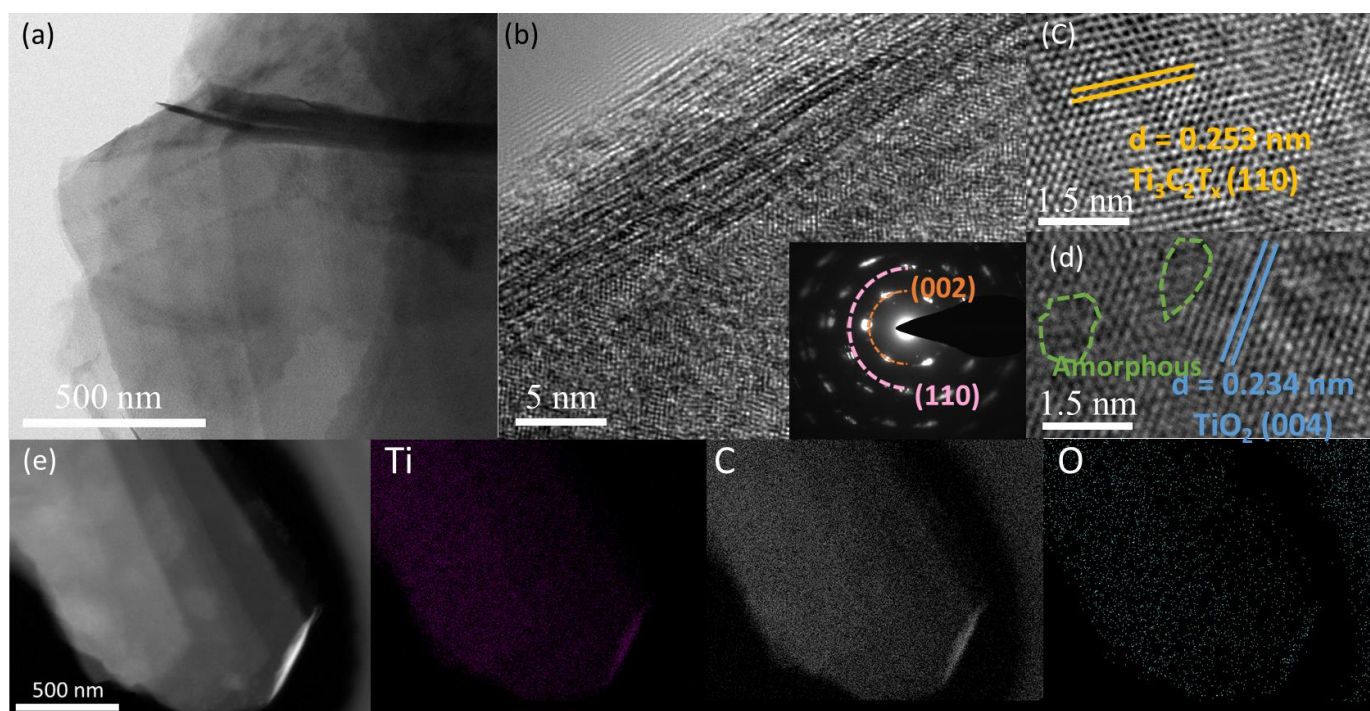**Figure 2.** (**a**) TEM image, (**b**) SAED pattern, (**c**,**d**) HR-TEM image, and (**e**) EDS mapping images of TiO_X-$Ti_3C_2T_X$.

The full XPS spectra of TiO_X-$Ti_3C_2T_X$ are shown in Figure 3a, there are obvious Ti, O, F, and C peaks in the TiO_X-$Ti_3C_2T_X$ curve, which indicates that after hydrothermal treatment, the unwanted Al-based impurities on the surface of MXene are completely removed and oxide passivation layers are successfully formed in situ. The Ti 2p spectra of TiO_X-$Ti_3C_2T_X$ (Figure 3b) could be well fitted into seven peaks. The peaks' centra at 455.3 and 462.6 eV are indexed to Ti-C and C-Ti-Fx bonding. The typical peak at 459.3 eV could be indexed to Ti-O, indicating the presence of a TiO_2 protective layer. Moreover, The C 1s spectra of TiO_X-$Ti_3C_2T_X$ (Figure 3c) show three peaks at 286.10, 284.80, and 282.70 eV, which correspond to C-O, C-C, and C-Ti, respectively. Besides, the characteristic peaks at 289.49 and 282.32 eV can be ascribed to COO/C-F and C-Ti-Tx bond in TiO_X-$Ti_3C_2T_X$ [40]. The O 1s spectra in Figure 3d can be well deconvoluted into two characteristic peaks. The obvious peaks located at 530.10 and 530.80 eV are related to the existence of lattice oxygen and O vacancy. Notably, the peak located at 532.28 eV could be ascribed to O-H. Besides, the intensity of the O-H peak is significantly larger than those of lattice oxygen peak and O vacancy peak, suggesting an enhanced functional-group coupling on the surface of Ti_3C_2, which is consistent with the previous FTIR data analysis. In general, after hydrothermal treatment, the surface of Ti_3C_2 formed a TiO_X protective layer with rich O vacancy and functional-groups with high activity, leading to higher electrochemical performance and stability.
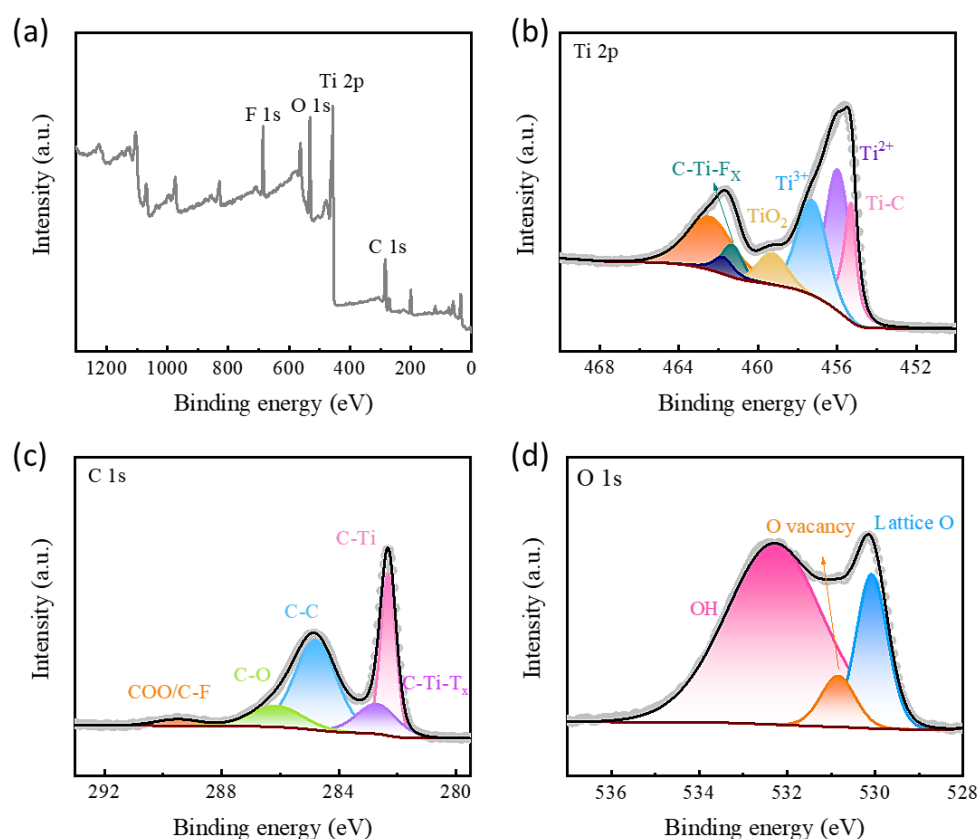
Figure 3. XPS surveys (**a**) and high-resolution Ti 2p (**b**), C 1s (**c**), O 1s (**d**) spectra for TiO_X-$Ti_3C_2T_X$.

The electrocatalytic activity of TiO_X-$Ti_3C_2T_X$ was examined as cathode in 2032-coin type LOBs. As shown in Figure 4a, the operating principle of Li-O_2 battery could be summarized as follows: O_2 (coming from the positive pole) can react with Li^+ (coming from the negative pole) to generate discharge product Li_2O_2 on the surface of the cathode in discharge, which could be fully decomposed after charging. As shown in Figure S3, the cyclic voltammetry (CV) curves of TiO_X-$Ti_3C_2T_X$-based cathode delivers a relatively high ORR onset potential (2.83 V) and a low OER onset potential (3.41 V), indicating a promising bifunctional oxygen catalytic performance. The initial full discharge/charge profiles of the LOBs assembled with TiO_X-$Ti_3C_2T_X$ at 2500 mA g^{-1} can be observed in Figure 4b. TiO_X-$Ti_3C_2T_X$ delivers a significantly remarkable discharge capacity of 7169 mAh g^{-1}. Especially, TiO_X-$Ti_3C_2T_X$ shows a low charge voltage platform, which is less than 4V during the limited specific capacity of 1000 mAh g^{-1}, which is favorable for improving the cycle efficiency, as well as extenuating the decomposition of the organic electrolyte. To explore the potential of TiO_X-$Ti_3C_2T_X$-based LOBs towards practical application, the full charge and discharge specific capacity of catalyst-based LOBs, normalized by the weight of actual electrodes (carbon paper + active materials), are presented in Figure S4. The LOBs based on TiO_X-$Ti_3C_2T_X$ in this work demonstrate a competitive specific capacity (639 mAh g^{-1}). Figure 4c shows the rate performance of TiO_X-$Ti_3C_2T_X$-based LOBs under different current densities. TiO_X-$Ti_3C_2T_X$ demonstrates a negligible difference in the discharge/charge curves when the applied current densities from 100 up to 2500 mA g^{-1} and then back to 100 mA g^{-1}. Notably, the LOB with TiO_X-$Ti_3C_2T_X$ shows relatively lower discharge–charge voltage gap even after high-rate charging and discharging. In detail, TiO_X-$Ti_3C_2T_X$ maintained a stable discharge–charge voltage gap from ~1.16 V at 100 mA g^{-1} to ~1.64 V at 2500 mA g^{-1}. Furthermore, TiO_X-$Ti_3C_2T_X$ shows little difference in the voltage curve after 50 cycling at 2500 mA g^{-1}, and delivering a stable voltage gap of ~1.72 V. Impressively, TiO_X-$Ti_3C_2T_X$ even sustained for almost 400 h and delivers low over-potential (~1.72 V) upon returning to low current density (100 mA g^{-1}). Circulation durability of

the as-prepared LOBs was measured at 2500 mA g^{-1} with a cut-off limited capacity of 1000 mAh g^{-1}. In Figure 4d, the TiO$_X$-Ti$_3$C$_2$T$_X$-based cathode can continuously sustain for 100 h (over 100 cycles) without distinct attenuation at ultra-high rate of 2500 mA g^{-1}, which is better than that of the Ti$_3$C$_2$T$_X$-based cathode. These indicate that the loading of TiO$_X$ protective layer and active functional-groups could significantly improve the electrochemical activity and stability of Ti$_3$C$_2$ MXene. The comparisons between recent reports and our work are listed in Table S2, regarding some key parameters such as first discharge capacity, cycling current density, and cycle stability. By comparison, the performance of the TiO$_X$-Ti$_3$C$_2$T$_X$-based cathode in this work is pretty good in LOBs.
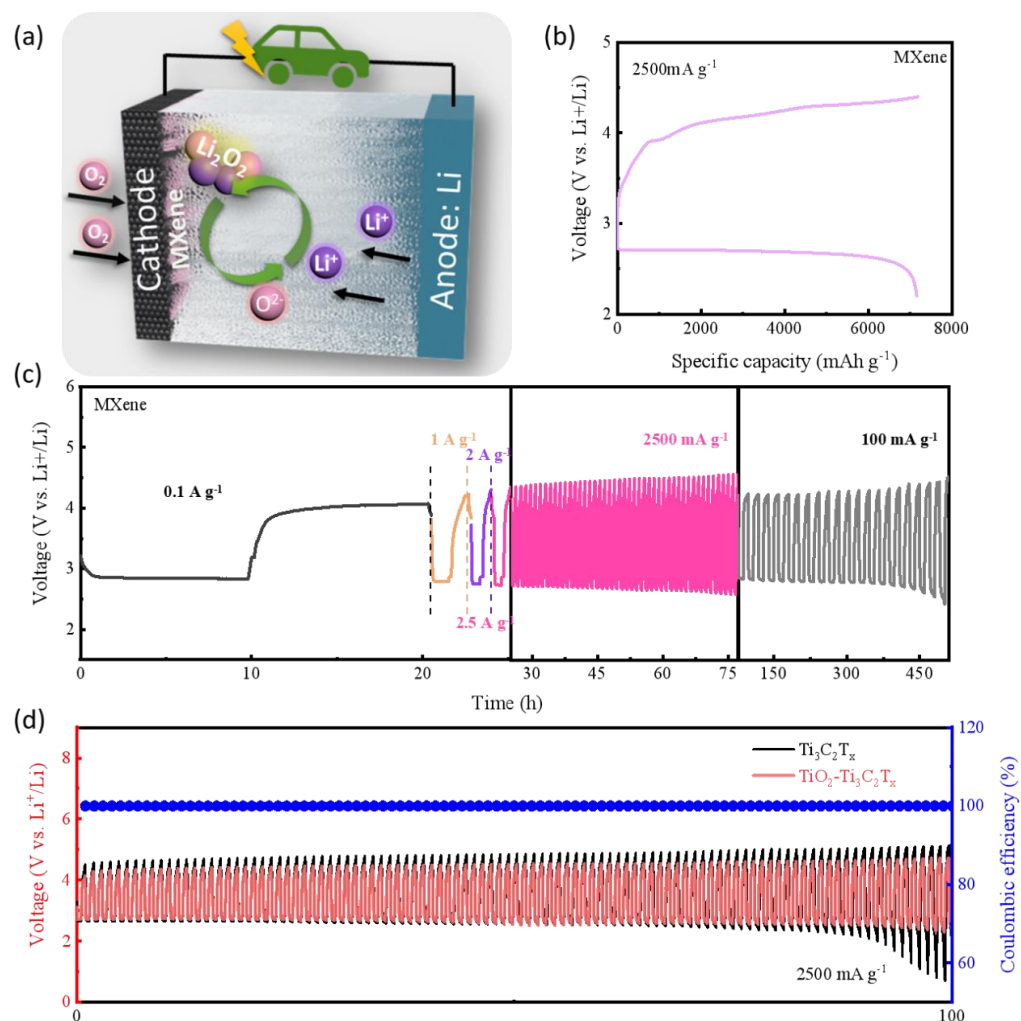

Figure 4. (**a**) Working mechanism of LOBs. (**b**) Initial full discharge/charge curves of TiO$_X$-Ti$_3$C$_2$T$_X$-based LOBs at 2500 mA g^{-1}; (**c**) rate performances of TiO$_X$-Ti$_3$C$_2$T$_X$-based LOBs; (**d**) cycling stability of as-prepared catalyst-based LOBs at 2500 mA g^{-1}.

To further analyze the catalytic mechanism of TiO$_X$-Ti$_3$C$_2$T$_X$, battery impedance after assembly, first discharge, and charge process have been tested by electrochemical impedance spectra (EIS) as shown in Figure 5. The as-prepared TiO$_X$-Ti$_3$C$_2$T$_X$ cathode delivers relevant ohmic resistance (Ro, 5.74 Ω) either after assembly or after the first cycle, but distinctly different charge transfer resistance (Rct). Typically, TiO$_X$-Ti$_3$C$_2$T$_X$-based LOBs showed higher Rct of 285.10 Ω after assembly than that of other stages. In detail, the TiO$_X$-Ti$_3$C$_2$T$_X$ cathode delivered Rct of 186.59 Ω after the first discharge and Rct of 91.40 Ω after the first discharge. The equivalent circuit shows that a new interface is formed on the surface of the cathode after discharge, which can be attributed to the formation of insoluble discharge products. By comparison, TiO$_X$-Ti$_3$C$_2$T$_X$ exhibited lower charge Rct values than

that of discharge, indicating that the TiO_X-$Ti_3C_2T_X$ could efficiently promote fast charge transfer kinetics and the decomposition of insoluble discharge products. Besides, the highest Rct values after assembly elucidated that the first electrochemical cycle reaction can effectively remove the impurities on the surface of TiO_X-$Ti_3C_2T_X$, which leads to reduced interface impedance and promotes the transmission of electrons.
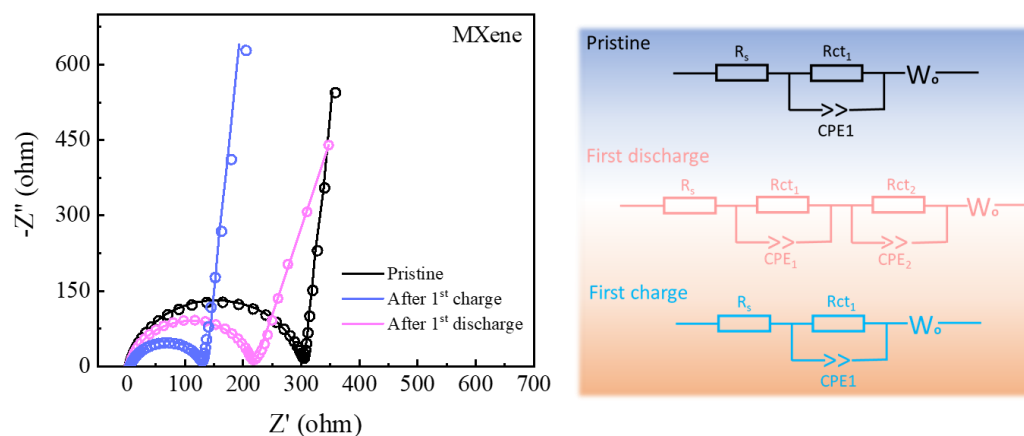

Figure 5. EIS of TiO_X-$Ti_3C_2T_X$-based LOBs after the 1st discharge-charge and their corresponding analog circuit diagram.

Although TiO_X-$Ti_3C_2T_X$ exhibits excellent electrochemical performance in LOBs, its stability still needs further optimization. Tailoring the surface functional groups could effectively improve the catalytic activity of $Ti_3C_2T_X$, which could also optimize the electronic properties. However, $Ti_3C_2T_X$ MXene is composed of mixed surface functional groups, which causes great disparity with the theoretical study. Therefore, theoretical analysis on mixed-functional groups of $Ti_3C_2T_X$ will be the next main research to clarify their effects in altering the electrochemical properties of $Ti_3C_2T_X$.

4. Conclusions

In conclusion, we creatively fabricated an in situ TiO_X protective layer on the surface of $Ti_3C_2T_X$ by a facile hydrothermal reaction. A TiO_X protective layer was adopted to directly optimize surface properties of $Ti_3C_2T_X$. The LOBs based on TiO_X-$Ti_3C_2T_X$ cathode exhibit superior specific capability (7169 mAh g^{-1}) and endurable stability at ultra-high rate (2500 mA g^{-1}). Such enhanced rate performances could be attributed to the three key aspects: (1) TiO_X behaves as in situ protective layer to optimize the structural stability of $Ti_3C_2T_X$, accompanied with enhancing the intensity of active functional-groups; (2) the uniformly-loaded active functional-groups (-F, -OH) could effectively optimize the catalytic performance of $TiO_X@Ti_3C_2T_X$; and (3) $TiO_X@Ti_3C_2T_X$ could promote fast charge transfer kinetics and the decomposition of insoluble discharge products. This work provides an efficient way to improve the stability and electrochemical activity of MXene catalysts for LOBs.

Author Contributions: Z.S., investigation, conceptualization, writing—original draft preparation; S.Z., data curation, methodology, supervision; J.Z., writing—review and editing, project administration. All authors have read and agreed to the published version of the manuscript.

Data Availability Statement: The data presented in this study are available on request from the corresponding author. The data are not publicly available due to privacy or ethical reasons.

Conflicts of Interest: We declare that the publication is approved by all authors and tacitly or explicitly by the responsible authorities where the work was carried out., there is no professional or other personal interest of any nature or kind in any product, service and company that could be construed as influencing the position presented in, or the review of, the manuscript entitled "High-conductive multilayer TiO_X-$Ti_3C_2T_X$ Electrocatalyst for Longevous Metal-Oxygen Battery under a High Rate".

References

1. Zhang, Z.; Ding, T.; Zhou, Q.; Sun, Y.; Qu, M.; Zeng, Z.; Ju, Y.; Li, L.; Wang, K.; Chi, F. A review of technologies and applications on versatile energy storage systems. *Renew. Sust. Energy Rev.* **2021**, *148*, 111263. [CrossRef]
2. Hussain, I.; Lamiel, C.; Sahoo, S.; Ahmad, M.; Chen, X.; Javed, M.S.; Qin, N.; Gu, S.; Li, Y.; Nawaz, T.; et al. Factors affecting the growth formation of nanostructures and their impact on electrode materials: A systematic review. *Mater. Today Phys.* **2022**, *27*, 100844. [CrossRef]
3. Liang, Y.; Chen, Y.; Ke, X.; Zhang, Z.; Wu, W.; Lin, G.; Zhou, Z.; Shi, Z. Coupling of triporosity and strong Au–Li interaction to enable dendrite-free lithium plating/stripping for long-life lithium metal anodes. *J. Mater. Chem. A* **2020**, *8*, 18094–18105. [CrossRef]
4. Balaish, M.; Jung, J.-W.; Kim, I.-D.; Ein-Eli, Y. A Critical Review on Functionalization of Air-Cathodes for Nonaqueous Li–O_2 Batteries. *Adv. Funct. Mater.* **2020**, *30*, 1808303. [CrossRef]
5. Cai, Y.; Zhang, Q.; Lu, Y.; Hao, Z.; Ni, Y.; Chen, J. An Ionic Liquid Electrolyte with Enhanced Li^+ Transport Ability Enables Stable Li Deposition for High-Performance Li-O_2 Batteries. *Angew. Chem. Int. Edit.* **2021**, *60*, 25973–25980. [CrossRef]
6. Cao, D.; Bai, Y.; Zhang, J.; Tan, G.; Wu, C. Irreplaceable carbon boosts Li-O_2 batteries: From mechanism research to practical application. *Nano Energy* **2021**, *89*, 106464. [CrossRef]
7. Cao, D.; Zheng, L.; Li, Q.; Zhang, J.; Dong, Y.; Yue, J.; Wang, X.; Bai, Y.; Tan, G.; Wu, C. Crystal Phase-Controlled Modulation of Binary Transition Metal Oxides for Highly Reversible Li–O_2 Batteries. *Nano Lett.* **2021**, *21*, 5225–5232. [CrossRef]
8. Liu, G.; Wang, N.; Qi, F.; Lu, X.; Liang, Y.; Sun, Z. Novel Ni–Ge–P anodes for lithium-ion batteries with enhanced reversibility and reduced redox potential. *Inorg. Chem. Front.* **2023**, *10*, 699–711. [CrossRef]
9. Hong, Y.-S.; Zhao, C.-Z.; Xiao, Y.; Xu, R.; Xu, J.-J.; Huang, J.-Q.; Zhang, Q.; Yu, X.; Li, H. Safe Lithium-Metal Anodes for Li-O_2 Batteries: From Fundamental Chemistry to Advanced Characterization and Effective Protection. *Batter. Supercaps* **2019**, *2*, 638–658. [CrossRef]
10. Hou, Y.; Wang, J.; Liu, J.; Hou, C.; Xiu, Z.; Fan, Y.; Zhao, L.; Zhai, Y.; Li, H.; Zeng, J.; et al. Interfacial Super-Assembled Porous CeO_2/C Frameworks Featuring Efficient and Sensitive Decomposing Li_2O_2 for Smart Li–O_2 Batteries. *Adv. Energy Mater.* **2019**, *9*, 1901751. [CrossRef]
11. Hu, Z.; Xie, Y.; Yu, D.; Liu, Q.; Zhou, L.; Zhang, K.; Li, P.; Hu, F.; Li, L.; Chou, S.; et al. Hierarchical $Ti_3C_2T_x$ MXene/Carbon Nanotubes for Low Overpotential and Long-Life Li-CO_2 Batteries. *ACS Nano* **2021**, *15*, 8407–8417. [CrossRef] [PubMed]
12. Jiang, Y.; Tian, M.; Wang, H.; Wei, C.; Sun, Z.; Rummeli, M.H.; Strasser, P.; Sun, J.; Yang, R. Mildly Oxidized MXene (Ti_3C_2, Nb_2C, and V_2C) Electrocatalyst via a Generic Strategy Enables Longevous Li–O_2 Battery under a High Rate. *ACS Nano* **2021**, *15*, 19640–19650. [CrossRef] [PubMed]
13. Lai, J.; Liu, H.; Xing, Y.; Zhao, L.; Shang, Y.; Huang, Y.; Chen, N.; Li, L.; Wu, F.; Chen, R. Local Strong Solvation Electrolyte Trade-Off between Capacity and Cycle Life of Li-O_2 Batteries. *Adv. Funct. Mater.* **2021**, *31*, 2101831. [CrossRef]
14. Li, J.; Ding, S.; Zhang, S.; Yan, W.; Ma, Z.-F.; Yuan, X.; Mai, L.; Zhang, J. Catalytic redox mediators for non-aqueous Li–O_2 battery. *Energy Storage Mater.* **2021**, *43*, 97–119. [CrossRef]
15. Li, M.; Wang, X.; Li, F.; Zheng, L.; Xu, J.; Yu, J. A Bifunctional Photo-Assisted Li–O_2 Battery Based on a Hierarchical Heterostructured Cathode. *Adv. Mater.* **2020**, *32*, 1907098. [CrossRef]
16. Li, N.; Wang, Y.; Peng, S.; Yuan, Y.; Wang, J.; Du, Y.; Zhang, W.; Han, K.; Ji, Y.; Dang, F. $Ti_3C_2T_x$ MXene cathode catalyst with efficient decomposition Li_2O_2 and high-rate cycle stability for Li-O_2 batteries. *Electrochim. Acta* **2021**, *388*, 138622. [CrossRef]
17. Liu, X.; Zhao, L.; Xu, H.; Huang, Q.; Wang, Y.; Hou, C.; Hou, Y.; Wang, J.; Dang, F.; Zhang, J. Tunable Cationic Vacancies of Cobalt Oxides for Efficient Electrocatalysis in Li–O2 Batteries. *Adv. Energy Mater.* **2020**, *10*, 2001415. [CrossRef]
18. McCloskey, B.D.; Scheffler, R.; Speidel, A.; Girishkumar, G.; Luntz, A.C. On the Mechanism of Nonaqueous Li–O_2 Electrochemistry on C and Its Kinetic Overpotentials: Some Implications for Li–Air Batteries. *J. Phys. Chem. C* **2012**, *116*, 23897–23905. [CrossRef]
19. Nam, S.; Mahato, M.; Matthews, K.; Lord, R.W.; Lee, Y.; Thangasamy, P.; Ahn, C.W.; Gogotsi, Y.; Oh, I.-K. Bimetal Organic Framework–$Ti_3C_2T_x$ MXene with Metalloporphyrin Electrocatalyst for Lithium–Oxygen Batteries. *Adv. Funct. Mater.* **2022**, *33*, 2210702. [CrossRef]

20. Peng, C.; Wei, P.; Li, X.; Liu, Y.; Cao, Y.; Wang, H.; Yu, H.; Peng, F.; Zhang, L.; Zhang, B.; et al. High efficiency photocatalytic hydrogen production over ternary $Cu/TiO_2@Ti_3C_2T_x$ enabled by low-work-function 2D titanium carbide. *Nano Energy* **2018**, *53*, 97–107. [CrossRef]

21. Plunkett, S.T.; Kondori, A.; Chung, D.Y.; Wen, J.; Wolfman, M.; Lapidus, S.H.; Ren, Y.; Amine, R.; Amine, K.; Mane, A.U.; et al. A New Cathode Material for a $Li–O_2$ Battery Based on Lithium Superoxide. *ACS Energy Lett.* **2022**, *7*, 2619–2626. [CrossRef]

22. Qiao, Y.; Wang, Q.; Mu, X.; Deng, H.; He, P.; Yu, J.; Zhou, H. Advanced Hybrid Electrolyte $Li–O_2$ Battery Realized by Dual Superlyophobic Membrane. *Joule* **2019**, *3*, 2986–3001. [CrossRef]

23. Song, S.; Yin, F.; Fu, Y.; Ren, J.; Ma, J.; Liu, Y.; Ma, R.; Ye, W. Simultaneous regulation of Li-ion intercalation and oxygen termination decoration on $Ti_3C_2T_x$ MXene toward enhanced oxygen electrocatalysis for $Li–O_2$ batteries. *Chem. Eng. J.* **2023**, *451*, 138818. [CrossRef]

24. Sun, Y.; Chen, K.; Zhang, C.; Yu, H.; Wang, X.; Yang, D.; Wang, J.; Huang, G.; Zhang, S. A Novel Material for High-Performance $Li–O_2$ Battery Separator: Polyetherketone Nanofiber Membrane. *Small* **2022**, *18*, 2201470. [CrossRef]

25. Sung, M.-C.; Lee, G.-H.; Kim, D.-W. Kinetic insight into perovskite $La_{0.8}Sr_{0.2}VO_3$ nanofibers as an efficient electrocatalytic cathode for high-rate $Li–O_2$ batteries. *InfoMat* **2021**, *3*, 1295–1310. [CrossRef]

26. Guo, S.; Wang, J.; Sun, Y.; Peng, L.; Li, C. Interface engineering of Co_3O_4/CeO_2 heterostructure in-situ embedded in Co/N-doped carbon nanofibers integrating oxygen vacancies as effective oxygen cathode catalyst for $Li–O_2$ battery. *Chem. Eng. J.* **2023**, *452*, 139317. [CrossRef]

27. Wang, D.; Mu, X.; He, P.; Zhou, H. Materials for advanced $Li–O_2$ batteries: Explorations, challenges and prospects. *Mater. Today* **2019**, *26*, 87–99. [CrossRef]

28. Abdul, M.; Mohd, Z.; Qasim, A.; Ahmed, M.; Ahmad, H.; Elsayed t El Fatimah, M.A.; Norah, S.A.; Shafaqat, A.; Muhammad, S.J. In Situ Nitrogen Functionalization of $2D-Ti_3C_2T_X$-MXenes for High-Performance Zn-Ion Supercapacitor. *Molecules* **2022**, *27*, 7446. [CrossRef]

29. Yan, Y.; Shu, C.; Zheng, R.; Li, M.; Ran, Z.; He, M.; Ren, L.; Du, D.; Zeng, Y. Long-cycling lithium-oxygen batteries enabled by tailoring Li nucleation and deposition via lithiophilic oxygen vacancy in $Vo-TiO_2/Ti_3C_2T_X$ composite anodes. *J. Energy Chem.* **2022**, *65*, 654–665. [CrossRef]

30. Wang, H.; Wang, X.; Li, M.; Zheng, L.; Guan, D.; Huang, X.; Xu, J.; Yu, J. Porous Materials Applied in Nonaqueous $Li–O_2$ Batteries: Status and Perspectives. *Adv. Mater.* **2020**, *32*, 2002559. [CrossRef] [PubMed]

31. Wang, H.; Zhao, N.; Bi, Z.; Gao, S.; Dai, Q.; Yang, T.; Wang, J.; Jia, Z.; Peng, Z.; Huang, J.; et al. Clear Representation of Surface Pathway Reactions at Ag Nanowire Cathodes in All-Solid $Li–O_2$ Batteries. *ACS Appl. Mater. Interfaces* **2021**, *13*, 39157–39164. [CrossRef] [PubMed]

32. Wang, H.; Zheng, R.; Shu, C.; Long, J. Promoting the Electrocatalytic Activity of $Ti_3C_2T_x$ MXene by Modulating CO_2 Adsorption through Oxygen Vacancies for High-Performance Lithium-Carbon Dioxide Batteries. *ChemElectroChem* **2020**, *7*, 4922–4930. [CrossRef]

33. Xiong, D.; Li, X.; Bai, Z.; Lu, S. Recent Advances in Layered $Ti_3C_2T_x$ MXene for Electrochemical Energy Storage. *Small* **2018**, *14*, 1703419. [CrossRef] [PubMed]

34. Xiong, Q.; Huang, G.; Yu, Y.; Li, C.-L.; Li, J.-C.; Yan, J.-M.; Zhang, X.-B. Soluble and Perfluorinated Polyelectrolyte for Safe and High-Performance $Li–O_2$ Batteries. *Angew. Chem. Int. Edit.* **2022**, *61*, e202116635. [CrossRef]

35. Yoo, E.; Zhou, H. LiF Protective Layer on a Li Anode: Toward Improving the Performance of $Li–O_2$ Batteries with a Redox Mediator. *ACS Appl. Mater. Interfaces* **2020**, *12*, 18490–18495. [CrossRef] [PubMed]

36. Zhang, J.; Kong, N.; Uzun, S.; Levitt, A.; Seyedin, S.; Lynch, P.A.; Qin, S.; Han, M.; Yang, W.; Liu, J.; et al. Scalable Manufacturing of Free-Standing, Strong $Ti_3C_2T_x$ MXene Films with Outstanding Conductivity. *Adv. Mater.* **2020**, *32*, 2001093. [CrossRef] [PubMed]

37. Zhang, Y.; Zhang, S.; Ma, J.; Huang, A.; Yuan, M.; Li, Y.; Sun, G.; Chen, C.; Nan, C. Oxygen Vacancy-Rich $RuO_2–Co_3O_4$ Nanohybrids as Improved Electrocatalysts for $Li–O_2$ Batteries. *ACS Appl. Mater. Interfaces* **2021**, *13*, 39239–39247. [CrossRef] [PubMed]

38. Zhao, N.; Zhang, F.; Zhan, F.; Yi, D.; Yang, Y.; Cui, W.; Wang, X. Fe^{3+}-stabilized $Ti_3C_2T_x$ MXene enables ultrastable Li-ion storage at low temperature. *J. Mater. Sci. Technol.* **2021**, *67*, 156–164. [CrossRef]

39. Zheng, R.; Shu, C.; Hou, Z.; Hu, A.; Hei, P.; Yang, T.; Li, J.; Liang, R.; Long, J. In Situ Fabricating Oxygen Vacancy-Rich TiO_2 Nanoparticles via Utilizing Thermodynamically Metastable Ti Atoms on $Ti_3C_2T_x$ MXene Nanosheet Surface To Boost Electrocatalytic Activity for High-Performance $Li–O_2$ Batteries. *ACS Appl. Mater. Interfaces* **2019**, *11*, 46696–46704. [CrossRef]

40. Zhou, Y.; Yin, K.; Gu, Q.; Tao, L.; Li, Y.; Tan, H.; Zhou, J.; Zhang, W.; Li, H.; Guo, S. Lewis-Acidic PtIr Multipods Enable High-Performance $Li–O_2$ Batteries. *Angew. Chem. Int. Edit.* **2021**, *60*, 26592–26598. [CrossRef]

41. Zheng, X.; Yuan, M.; Guo, D.; Wen, C.; Li, X.; Huang, X.; Li, H.; Sun, G. Theoretical Design and Structural Modulation of a Surface-Functionalized $Ti_3C_2T_x$ MXene-Based Heterojunction Electrocatalyst for a Li–Oxygen Battery. *ACS Nano* **2022**, *16*, 4487–4499. [CrossRef]

42. Lu, Y.; Ang, H.; Yan, Q.; Fong, E. Bioinspired Synthesis of Hierarchically Porous MoO_2/Mo_2C Nanocrystal Decorated N-Doped Carbon Foam for Lithium–Oxygen Batteries. *Chem. Mater.* **2016**, *28*, 5743–5752. [CrossRef]

43. Liu, J.; Li, D.; Wang, Y.; Zhang, S.; Kang, Z.; Xie, H.; Sun, L. MoO_2 nanoparticles/carbon textiles cathode for high performance flexible Li-O$_2$ battery. *J. Energy Chem.* **2020**, *47*, 66–71. [CrossRef]

44. Cao, X.; Sun, Z.; Zheng, X.; Jin, C.; Tian, J.; Li, X.; Yang, R. $MnCo_2O_4/MoO_2$ Nanosheets Grown on Ni foam as Carbon- and Binder-Free Cathode for Lithium–Oxygen Batteries. *ChemSusChem* **2018**, *11*, 574–579. [CrossRef]